



Semnan University

Mechanics of Advanced Composite Structures

journal homepage: <http://MACS.journals.semnan.ac.ir>

Free Vibration Analysis of Size-Dependent Multi-Layered Graphene Sheets Based on Strain Gradient Elasticity Theory

K. Khorshidi ^{a,b*}, M. Karimi ^a, A.A. Alinezhad ^a^a Department of Mechanical Engineering, Arak University, Arak, 38156-88349, Iran^b Institute of Nanosciences & Nanotechnology, Arak University, Arak, 38156-88349, Iran

KEYWORDS

Navier method;
ESDT;
Multi-layered graphene sheets;
Strain Gradient Theory.

ABSTRACT

This study investigates the size-dependent free vibration analysis of multi-layered graphene sheets based on exponential shear deformation theory (ESDT), which considers the effects of rotary inertia and transverse shear deformations. In order to capture the effects of length scale parameter on the vibrational behavior of the structure, modified strain gradient elasticity theory is utilized. An elastic multiple-plate model is assumed in which the nested plates are coupled with each other through the van der Waals interlayer forces. The governing equations of motion are derived by implementing Hamilton's principle and then are solved with the Navier approach. To verify the present model, results in specific cases are compared with the available papers in the literature and excellent agreement is seen. Finally, the effects of various parameters such as aspect ratio, thickness ratio, Winkler modulus, shear modulus, and size effects on the natural frequencies of a multi-layered graphene sheet are presented and discussed in detail.

1. Introduction

Carbon nanotubes (CNTs), graphene sheets (GSs), and fullerenes are the principal elements of carbon nanostructures, which caused a considerable promotion in the world of nanotechnology. Graphene is a two-dimensional atomic crystal with special electronic and mechanical properties. Graphene sheets are useful structures in polymer composites in order to strengthen them. Moreover, thanks to their extraordinary features, graphene sheets are widely utilized in various systems such as biomedical employment, nano-mechanical devices, solar cells, etc. Multi-layered graphene sheets that are held together by van der Waals interactions have received a great deal of attention to the scientific community, as the bending stiffness of the multi-layered graphene sheet is usually more than single-layered graphene sheet.

Experiments have shown that the small-scale effect has a major role in the analysis of small-scale structures and cannot be ignored [1-13]. Atomic simulations and continuum mechanics are common methods for modeling a structure in small scales. In contrary to atomic

simulations, continuum mechanics are computationally expensive. Hence, researchers are interested in continuum mechanics to analyze the behavior of systems in small scales. Additionally, classical theories are not capable to capture the mechanical behavior response of micro and nano-sized structures since they do not include any length scale parameters. Various size-dependent continuum models such as the modified couple stress theory [14-17], the nonlocal elasticity theory [18-22] and the strain gradient theory [23] can be used in small-scale systems. Strain gradient theory as a recognized theory for analysis of size-dependent behavior includes five independent length scale parameters and considers strain energy of the second-order gradient of deformations. Lam et al. [24] developed the strain gradient theory and assumed only three length-scale parameters to catch the scale effects. Their modified strain gradient theory contains a new additional equilibrium equation as well as the classical equilibrium equations.

In recent years, reinforced structures like graphene sheets have been studied extensively [25-30]. Ansari et al. [31] investigated the vibrational characteristics of multi-layered

* Corresponding author. Tel.: +98-86-32625720 ; Fax: +98-86-32625721
E-mail address: k-khorshidi@araku.ac.ir

graphene sheets with various boundary conditions based on the Mindlin plate theory, and the Eringen nonlocal elasticity. In their study, the nested nanoplates interacted with each other through the van der Waals interactions between all the layers. Sobhy [32] studied a two-variable plate theory with a sinusoidal distribution for transverse shear stress in order to analyze the vibration of the orthotropic double-layered graphene sheets in the hydrothermal environment. Wang et. al. [33] studied the vibration of double-layered nanoplates in the thermal environment. They considered small-scale effects using the nonlocal continuum theory and concluded that nonlocal effects are more prominent at larger half wave numbers. Shafiei et. al. [34] conducted a study on the size-dependent vibration and buckling of multi-layered graphene sheets using couple stress theory, which is a special case of strain gradient theory. They adopted a modified plate theory with only two variables with the help of the finite strip approach to formulate their model. Karličić et. al. [35] investigated the stability analysis and thermal vibration of multi-layer graphene sheets (MLGS) embedded in an elastic medium based on the nonlocal Kirchhoff-Love plate theory. They applied Navier's method to find the exact closed-form solution for natural frequencies and critical buckling loads of the structure. Kitipornchai et. al. [36] analyzed the vibration of simply-supported MLGSs based on a continuum model. They concluded that vibration modes related to the classical natural frequencies are similar in amplitude and direction while vibration modes of resonant frequencies are different because of the van der Waals interactions. Hosseini Hashemi et. al. [37] studied the free vibration analysis of double viscoelastic graphene sheets coupled with a Visco-Pasternak layer based on the classical plate theory. They employed the Kelvin-Voigt model and presented an exact solution for governing equations. He et. al. [38] investigated the stability of the multi-walled carbon nanotubes with an efficient algorithm. They assumed individual tubes as continuum cylindrical shells and considered van der Waals (vdW) interactions as a constant, which is independent of the tubes' radius. Ansari et. al. [39] presented a numerical solution using the differential quadrature method for vibration analysis of embedded multi-layered graphene sheets with various boundary conditions based on the Mindlin theory. Radić and Jeremić [40] utilized the Galerkin approach for buckling and vibration of Mindlin orthotropic double-layered graphene sheets subjected to hygrothermal loading for seven different boundary conditions based on a nonlocal elasticity model.

Nazemnezhad et. al. [41] studied the essence of nonlocal elasticity for vibration analysis of multi-layer graphene sheets based on the sandwich model. They compared their results with Molecular Dynamic (MD) simulation and concluded that the van der Waals interactions result in the interlayer shear effect. Arefi et. al. [42] demonstrated the nonlocal dynamic behavior of three-layered nanoplates with piezomagnetic face sheets resting on Pasternak's foundation based on first-order shear deformation theory. In their research work, the Navier method was used to solve the governing equations.

In the present work, the exponential shear deformable plate theory (ESDPT) in conjunction with strain gradient elasticity is employed to study the effects of the material length scale parameters on the vibrational behavior of multi-layered graphene sheets. The governing partial differential equations are obtained using Hamilton's principle, and then the Navier solution is presented to analyze the free vibration of simply supported graphene sheets. The elastic foundation is considered to be Pasternak. To validate the presented method, our results are compared to those in the corresponding literature. The results of the present work can be used as benchmarks for future works.

2. Formulation

Consider a multi-layered graphene sheet embedded in an elastic medium with length a , width b , mass density ρ , and constant thickness h , as shown in Figure 1.

To study the motion of the graphene sheet, a coordinate system is located in the corner of the structure. The displacement field according to the exponential shear deformation plate theory for each layer of MLGS can be written as [20]

$$u^{(i)}(x, y, z, t) = u_0^{(i)}(x, y, z, t) - z \frac{\partial w^{(i)}(x, y, t)}{\partial x} + f(z)\phi^{(i)}(x, y, t) \quad (1)$$

$$v^{(i)}(x, y, z, t) = v_0^{(i)}(x, y, z, t) - z \frac{\partial w^{(i)}(x, y, t)}{\partial y} + f(z)\psi^{(i)}(x, y, t) \quad (2)$$

$$W^{(i)}(x, y, z, t) = w^{(i)}(x, y, t) \quad (3)$$

where $f(z) = z \left(e^{-2\left(\frac{z}{h}\right)^2} \right)$ and $f(z) = \frac{h}{\pi} \sin\left(\frac{\pi z}{h}\right)$ for exponential (ESDT) and trigonometric theory (TSDT), respectively.

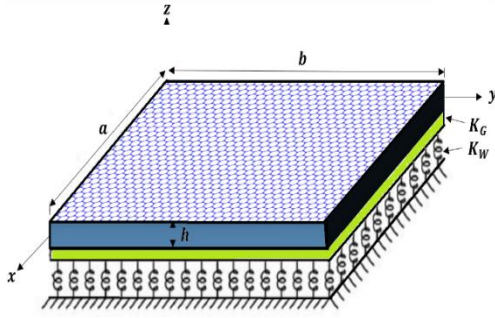


Figure 1. Rectangular multilayered nano-graphene sheet embedded in an elastic medium

In Eqs. (1)-(3), $u^{(i)}$, $v^{(i)}$ and $W^{(i)}$ denote the displacement of an arbitrary point in the x, y, and z directions for the i-th sheet of the MLGS, respectively. $u_0^{(i)}$ and $v_0^{(i)}$ are the mid-plane displacements, and $\phi^{(i)}$ and $\psi^{(i)}$ express the rotation functions.

The strain energy of the structure with volume Ω can be written as [2]

$$U^{(i)} = \int_{\Omega} (\sigma_{ij} \delta \epsilon_{ij} + m_{ij} \delta \chi_{ij} + P_i \delta \gamma_i + \tau_{ijk} \delta \eta_{ijk}) d\Omega \tag{4}$$

where the deformation functions can be defined as below:

$$\epsilon_{ij} = \frac{1}{2} (u_{i,j} + u_{j,i}), \quad i, j = x, y, z \tag{5}$$

$$\gamma_i = \epsilon_{mm,i} \tag{6}$$

$$\eta_{ijk} = \frac{1}{3} (\epsilon_{jk,i} + \epsilon_{ki,j} + \epsilon_{ij,k}) - \frac{1}{15} \delta_{ij} (\epsilon_{mm,i} + 2\epsilon_{mk,m}) - \frac{1}{15} [\delta_{jk} (\epsilon_{mm,i} + 2\epsilon_{mi,m}) + \delta_{ki} (\epsilon_{mm,j} + 2\epsilon_{mj,m})] \tag{7}$$

$$\chi_{ij} = \frac{1}{2} e_{ijk} u_{j,ki} \tag{8}$$

in which u_i is the displacement vector in the direction of i (i=x, y, z). ϵ_{ij} , $\epsilon_{mm,i}$, η_{ijk} and χ_{ij} denote the strain tensor, the dilation gradient vector, deviatoric stretch gradient tensor and the symmetric rotation gradient tensor, respectively. Moreover, δ_{ki} is the Kronecker delta and e_{ijk} represents the permutation symbol, which can be expressed as follows:

$$e_{ijk} = \begin{cases} 1 & \text{for a forward permutation of } ijk \\ -1 & \text{for a backward permutation of } ijk \\ 0 & \text{if } i, j \text{ or } k \text{ are equal} \end{cases}$$

σ_{ij} indicates the classical stress tensor and P_i , τ_{ijk} , m_{ij} are stress measures for the higher order stresses, which can be written as follows[2]:

$$\sigma_{ij} = \lambda \epsilon_{mm} \delta_{ij} + 2\mu \epsilon'_{ij} \tag{9}$$

$$P_i = 2\mu l_0^2 \gamma_i \tag{10}$$

$$\tau_{ijk} = 2\mu l_1^2 \eta_{ijk} \tag{11}$$

$$m_{ij} = 2\mu l_2^2 \chi_{ij} \tag{12}$$

$$\epsilon'_{ij} = \epsilon_{ij} - \frac{1}{3} \epsilon_{mm} \delta_{ij} \tag{13}$$

in which l_0, l_1, l_2 are material length scale parameters related to dilatation gradients, deviatoric stretch gradients, and rotation gradients respectively. Also, λ and μ are Lamé constants that can be expressed in the following form:

$$\lambda = \frac{\nu E}{(1 + \nu)(1 - 2\nu)} \tag{14}$$

$$\mu = \frac{E}{2(1 + \nu)} \tag{15}$$

where E is Young's modulus and ν is Poisson's ratio. Considering Hooke's Law for the stress field, the normal stress σ_{zz} is assumed to be negligible in comparison with plane stresses σ_{xx} and σ_{yy} . Thus, stress and strain fields can be related as below

$$\sigma_{xx} = \frac{E}{1 - \nu^2} (\epsilon_{xx} + \nu \epsilon_{yy}) \tag{16}$$

$$\sigma_{yy} = \frac{E}{1 - \nu^2} (\epsilon_{yy} + \nu \epsilon_{xx}) \tag{17}$$

$$\sigma_{xy} = 2G \epsilon_{xy} \tag{18}$$

$$\sigma_{xz} = 2G \epsilon_{xz} \tag{19}$$

$$\sigma_{yz} = 2G \epsilon_{yz} \tag{20}$$

where $G = E/2(1 + \nu)$ is the shear modulus of the structure. The kinetic energy $K^{(i)}$ and the work done by the external applied forces $W^{(i)}$ related to the i-th layer of an N-layered GS can be written as

$$K^{(i)} = \int_{\Omega} \rho (u \dot{u} + v \dot{v} + w \dot{w}) d\Omega, \tag{21}$$

$$W^{(i)} = \int_A \left(\bar{P}_i + \bar{K}_G \left(\frac{\partial^2 w}{\partial x^2} + \frac{\partial^2 w}{\partial y^2} \right) \right) \delta w dx dy, \tag{22}$$

where dot-superscript denotes the differentiation with respect to the time variable t. Also, K_G is shear modulus and \bar{P}_i is the pressure exerted on the i-th layer through the van der Waals interaction forces and the surrounding elastic medium, which are defined as follows:

$$\bar{P}_i = (P_{vdw})_i + (\delta_{i1} + \delta_{iN})(P_{Winkler})_i \tag{23}$$

$$\delta_{i1} = \begin{cases} 0, & i \neq j \\ 1, & i = j \end{cases}$$

In Eq. (23), $(P_{vdw})_i$ indicates the pressure exerted on the i-th layer due to the van der Waals interaction of the remaining layers and can be given as

$$(P_{vdw})_i = W_i \sum_{j=1}^N C_{ij} - \sum_{j=1}^N C_{ij} W_j \tag{24}$$

(i = 1,2,3,...,N)

where the van der Waals coefficients C_{ij} represent the rising pressure to the i -th layer from the j -th layer and are given as follows [31]:

$$C_{ij} = - \left(\frac{4\sqrt{3}}{9a} \right)^2 \frac{24\epsilon}{\sigma^2} \left(\frac{\sigma}{a_{cc}} \right)^8 \frac{3003\pi}{256} \sum_{k=0}^5 \frac{(-1)^k}{2k+1} \tag{25}$$

$$(5) \left(\frac{\sigma}{a_{cc}} \right)^6 \frac{1}{h_{ij}^2} - \left(\frac{35\pi}{8} \right)^8 \left[\sum_{k=0}^5 \frac{(-1)^k}{2k+1} \frac{1}{h_{ij}^{2k}} \right]$$

where a_{cc} and h_{ij} denote the length of carbon-carbon bond and the distance between two layers, respectively. Moreover, σ and ϵ are two parameters relating to the carbon-carbon bond. The van der Waals interaction coefficients C_{ij} are calculated using equation (25) and are expressed in Table 1 for a ten-layered GS. Note that the negative sign in Table 1 shows an attraction between two layers while the positive sign shows repulsion. According to this table, the van der Waals interaction coefficient C_{ij} between two adjacent layers is the largest coefficient, which indicates that the van der Waals interaction of two adjacent layers is the strongest interaction [31]. Moreover, it is seen that the van der Waals interaction decreases

considerably as the distance between two layers increases.

It is worth mentioning that $(P_{Winkler})_i$ in Eq. (23) is the Winkler foundation model which can be expressed as [32];

$$(P_{Winkler})_i = -\bar{K}_w W_i, \quad (i = 1, \dots, N) \tag{26}$$

in which K_w is the Winkler modulus, which depends on the material properties of the elastic medium. Implementing Hamilton's principle, the governing equations of the Multi-layered graphene sheets can be derived as follows [37]

$$\int_0^T (\delta U + \delta W - \delta K) dt = 0, \tag{27}$$

where U , K , and W express strain energy, kinetic energy, and work done by external forces, respectively. Besides, δ is a variation operator. The governing equations for the i -th layer of an N -layered GS can be obtained by incorporating Eqs. (4), (21), and (22) into Eq. (27) and then using integrating by parts and setting the coefficients of $\delta u_0^{(i)}, \delta v_0^{(i)}, \delta w^{(i)}, \delta \phi^{(i)}$ and $\delta \psi^{(i)}$ to zero as follows

$$\delta u_0^{(i)}: \frac{\partial N_{xx}}{\partial x} + \frac{\partial N_{xy}}{\partial y} + \frac{1}{2} \frac{\partial^2 N_{xz}^m}{\partial x \partial y} + \frac{1}{2} \frac{\partial^2 N_{yz}^m}{\partial y^2} - \left(\frac{2}{5} \frac{\partial^2 R_{xxx}}{\partial x^2} - \frac{1}{5} \frac{\partial^2 R_{xxx}}{\partial y^2} + \frac{8}{15} \frac{\partial^2 R_{xxy}}{\partial x \partial y} + \frac{8}{15} \frac{\partial^2 R_{xyy}}{\partial x \partial y} + \frac{4}{15} \frac{\partial^2 R_{xyy}}{\partial y^2} - \frac{1}{5} \frac{\partial^2 R_{xxy}}{\partial x^2} - \frac{1}{5} \frac{\partial^2 R_{xzz}}{\partial x^2} - \frac{1}{15} \frac{\partial^2 R_{xzz}}{\partial y^2} + \frac{8}{15} \frac{\partial^2 R_{yxx}}{\partial x \partial y} + \frac{4}{15} \frac{\partial^2 R_{yxy}}{\partial y^2} - \frac{1}{5} \frac{\partial^2 R_{yxy}}{\partial x^2} + \frac{4}{15} \frac{\partial^2 R_{yyx}}{\partial y^2} - \frac{1}{5} \frac{\partial^2 R_{yyx}}{\partial x^2} - \frac{2}{5} \frac{\partial^2 R_{yyy}}{\partial x \partial y} - \frac{2}{5} \frac{\partial^2 R_{yzz}}{\partial x \partial y} - \frac{1}{5} \frac{\partial^2 R_{zxx}}{\partial x^2} - \frac{1}{15} \frac{\partial^2 R_{zxx}}{\partial y^2} - \frac{2}{15} \frac{\partial^2 R_{zzy}}{\partial x \partial y} \right) - \left(\frac{\partial^2 N_x^p}{\partial x^2} + \frac{\partial^2 N_y^p}{\partial x \partial y} \right) - \bar{P} = I_0 \frac{\partial^2 u_0}{\partial t^2} - I_1 \frac{\partial^3 w}{\partial x \partial t^2} + I_3 \frac{\partial^2 \phi}{\partial t^2}, \tag{28}$$

$$\delta v_0^{(i)}: \frac{\partial N_{yy}}{\partial y} + \frac{\partial N_{xy}}{\partial x} - \frac{1}{2} \frac{\partial^2 N_{xz}^m}{\partial x \partial y} - \left(-\frac{2}{5} \frac{\partial^2 R_{xxx}}{\partial x \partial y} + \frac{4}{15} \frac{\partial^2 R_{xxy}}{\partial x^2} - \frac{1}{5} \frac{\partial^2 R_{xxy}}{\partial y^2} + \frac{4}{15} \frac{\partial^2 R_{xyx}}{\partial x^2} - \frac{1}{5} \frac{\partial^2 R_{xyx}}{\partial y^2} + \frac{8}{15} \frac{\partial^2 R_{xyy}}{\partial x \partial y} - \frac{2}{15} \frac{\partial^2 R_{xzz}}{\partial x \partial y} + \frac{4}{15} \frac{\partial^2 R_{yxx}}{\partial x^2} + \frac{8}{15} \frac{\partial^2 R_{xxy}}{\partial x \partial y} - \frac{2}{15} \frac{\partial^2 R_{xzz}}{\partial y^2} + \frac{4}{15} \frac{\partial^2 R_{yxx}}{\partial x^2} - \frac{1}{5} \frac{\partial^2 R_{yxx}}{\partial y^2} - \frac{1}{5} \frac{\partial^2 R_{yxx}}{\partial x^2} + \frac{8}{15} \frac{\partial^2 R_{yyx}}{\partial x \partial y} + \frac{8}{15} \frac{\partial^2 R_{yyx}}{\partial y^2} + \frac{2}{5} \frac{\partial^2 R_{yyy}}{\partial x \partial y} - \frac{1}{5} \frac{\partial^2 R_{yzz}}{\partial x^2} - \frac{1}{5} \frac{\partial^2 R_{yzz}}{\partial y^2} - \frac{2}{15} \frac{\partial^2 R_{zxx}}{\partial x \partial y} - \frac{1}{5} \frac{\partial^2 R_{zxx}}{\partial y^2} - \frac{2}{15} \frac{\partial^2 R_{zzy}}{\partial x \partial y} - \frac{1}{5} \frac{\partial^2 R_{zzy}}{\partial x^2} \right) - \left(\frac{\partial^2 N_x^p}{\partial x \partial y} + \frac{\partial^2 N_y^p}{\partial y^2} \right) = I_0 \frac{\partial^2 v_0}{\partial t^2} - I_1 \frac{\partial^3 w}{\partial y \partial t^2} + I_3 \frac{\partial^2 \psi}{\partial t^2}, \tag{29}$$

$$\delta W(i): \frac{\partial^2 M_{xx}}{\partial x^2} + 2 \frac{\partial^2 M_{xy}}{\partial x \partial y} + \frac{\partial^2 M_{yy}}{\partial y^2} + \frac{\partial^2 M_{yy}}{\partial y^2} - \frac{\partial^2 N_{xx}^m}{\partial x \partial y} + \frac{\partial^2 N_{yy}^m}{\partial x \partial y} - \frac{\partial^2 N_{xy}^m}{\partial y^2} + \frac{\partial^2 N_{xy}^m}{\partial x^2} + \left(-\frac{2}{5} \frac{\partial^3 R_{xxx}^z}{\partial x^3} + \frac{3}{5} \frac{\partial^3 R_{xxx}^z}{\partial x \partial y^2} - \frac{4}{5} \frac{\partial^3 R_{xxy}^z}{\partial y \partial x^2} + \frac{1}{5} \frac{\partial^3 R_{xxy}^z}{\partial y^3} + \frac{4}{15} \frac{\partial^3 R_{xzz}^z}{\partial x^2} - \frac{1}{15} \frac{\partial^3 R_{xzz}^z}{\partial y^2} - \frac{4}{5} \frac{\partial^3 R_{xyx}^z}{\partial y \partial x^2} + \frac{1}{5} \frac{\partial^3 R_{xyx}^z}{\partial y^3} - \frac{4}{5} \frac{\partial^3 R_{xyy}^z}{\partial x \partial y^2} + \frac{1}{5} \frac{\partial^3 R_{xyy}^z}{\partial x^3} + \frac{1}{3} \frac{\partial^2 R_{xyz}}{\partial x \partial y} + \frac{4}{15} \frac{\partial^2 R_{xxx}}{\partial x^2} - \frac{1}{15} \frac{\partial^2 R_{xxx}}{\partial y^2} + \frac{1}{3} \frac{\partial^2 R_{xzy}}{\partial x \partial y} + \frac{1}{5} \frac{\partial^3 R_{xzz}^z}{\partial x^3} + \frac{1}{5} \frac{\partial^3 R_{xzz}^z}{\partial x \partial y^2} - \frac{4}{5} \frac{\partial^3 R_{yxx}^z}{\partial y \partial x^2} + \frac{1}{5} \frac{\partial^3 R_{yxx}^z}{\partial y^3} - \frac{4}{5} \frac{\partial^3 R_{yxy}^z}{\partial x \partial y^2} + \frac{1}{5} \frac{\partial^3 R_{yxy}^z}{\partial x^3} + \frac{1}{5} \frac{\partial^2 R_{yzz}}{\partial x \partial y} - \frac{4}{5} \frac{\partial^3 R_{yzz}^z}{\partial x \partial y^2} + \frac{1}{5} \frac{\partial^3 R_{yzz}^z}{\partial y^3} + \frac{3}{5} \frac{\partial^3 R_{yzy}^z}{\partial y \partial x^2} + \frac{4}{5} \frac{\partial^2 R_{yyz}}{\partial y^2} - \frac{1}{15} \frac{\partial^2 R_{yyz}}{\partial x^2} + \frac{1}{3} \frac{\partial^2 R_{yyz}}{\partial x \partial y} + \frac{4}{15} \frac{\partial^2 R_{yzy}}{\partial x \partial y} + \frac{1}{5} \frac{\partial^2 R_{yzz}}{\partial x^2} + \frac{1}{5} \frac{\partial^2 R_{yzz}}{\partial y^2} + \frac{1}{5} \frac{\partial^3 R_{zxx}^z}{\partial x^3} - \frac{1}{15} \frac{\partial^3 R_{zxx}^z}{\partial x \partial y^2} + \frac{1}{3} \frac{\partial^3 R_{zxx}^z}{\partial x \partial y} + \frac{1}{5} \frac{\partial^3 R_{zxx}^z}{\partial x^3} + \frac{1}{5} \frac{\partial^3 R_{zxx}^z}{\partial x \partial y^2} + \frac{1}{3} \frac{\partial^2 R_{zyx}}{\partial x \partial y} + \frac{4}{15} \frac{\partial^2 R_{zyy}}{\partial y^2} - \frac{1}{15} \frac{\partial^2 R_{zyy}}{\partial x^2} + \frac{1}{5} \frac{\partial^3 R_{zyz}^z}{\partial y \partial x^2} + \frac{1}{5} \frac{\partial^3 R_{zyz}^z}{\partial y^3} + \frac{1}{5} \frac{\partial^3 R_{zyz}^z}{\partial x^3} + \frac{1}{5} \frac{\partial^3 R_{zyz}^z}{\partial x \partial y^2} + \frac{1}{5} \frac{\partial^3 R_{zyz}^z}{\partial y^3} - \frac{1}{5} \frac{\partial^2 R_{zzz}}{\partial x^2} - \frac{1}{5} \frac{\partial^2 R_{zzz}}{\partial y^2} \right) - \left(\frac{\partial^3 N_x^p}{\partial x^3} + \frac{\partial^3 N_x^p}{\partial x \partial y^2} + \frac{\partial^3 N_y^p}{\partial y \partial x^2} + \frac{\partial^3 N_y^p}{\partial y^3} - \frac{\partial^2 N_z^p}{\partial x^2} - \frac{\partial^2 N_z^p}{\partial y^2} \right) + \bar{P}_l - K_G \left(\frac{\partial^2 w}{\partial x^2} + \frac{\partial^2 w}{\partial y^2} \right) = I_0 \frac{\partial^2 w}{\partial t^2} + I_1 \left(\frac{\partial^3 u_0}{\partial x \partial t^2} + \frac{\partial^3 v_0}{\partial y \partial t^2} \right) - I_2 \left(\frac{\partial^4 w}{\partial x^2 \partial t^2} + \frac{\partial^4 w}{\partial y^2 \partial t^2} \right) I_4 \left(\frac{\partial^3 \phi}{\partial x \partial t^2} + \frac{\partial^3 \psi}{\partial y \partial t^2} \right) \tag{30}$$

$$\delta\phi^{(i)}: \frac{\partial N_{xx}^f}{\partial x} + \frac{\partial N_{xy}^f}{\partial y} - Q_x + \frac{1}{2} \frac{\partial N_{yy}^{mdf}}{\partial y} + \frac{1}{2} \frac{\partial N_{xy}^{mdf}}{\partial x} + \frac{1}{2} \frac{\partial^2 N_{xz}^{mf}}{\partial y \partial x} + \frac{1}{2} \frac{\partial^2 N_{yz}^{mf}}{\partial y^2} - \frac{1}{2} N_{yz}^{mddf} + \left(-\frac{2}{5} \frac{\partial^2 R_{xxx}^f}{\partial x^2} + \frac{1}{5} \frac{\partial^2 R_{xxx}^f}{\partial y^2} + \frac{1}{5} R_{xxx}^{ddf} - \frac{8}{15} \frac{\partial^2 R_{xxy}^f}{\partial y \partial x} + \frac{8}{15} \frac{\partial^2 R_{xxx}^f}{\partial x^2} - \frac{8}{15} \frac{\partial^2 R_{xyx}^f}{\partial y \partial x} - \frac{4}{15} \frac{\partial^2 R_{xyy}^f}{\partial y^2} + \frac{1}{5} \frac{\partial^2 R_{xyy}^f}{\partial x^2} + \frac{1}{15} R_{xyy}^{ddf} + \frac{1}{3} \frac{\partial R_{xyz}^{df}}{\partial y} + \frac{8}{15} \frac{\partial R_{zxx}^{df}}{\partial x} + \frac{1}{3} \frac{\partial R_{xzy}^{df}}{\partial y} - \frac{4}{15} R_{xzz}^{ddf} + \frac{1}{5} \frac{\partial^2 R_{xzz}^f}{\partial x^2} + \frac{1}{15} \frac{\partial^2 R_{xzz}^f}{\partial y^2} - \frac{8}{15} \frac{\partial^2 R_{yxx}^f}{\partial y \partial x} - \frac{4}{15} \frac{\partial^2 R_{yxy}^f}{\partial y^2} + \frac{1}{5} \frac{\partial^2 R_{yxy}^f}{\partial x^2} + \frac{1}{15} R_{yxy}^{ddf} + \frac{1}{3} \frac{\partial R_{yxz}^{df}}{\partial y} - \frac{4}{15} \frac{\partial^2 R_{yyx}^f}{\partial y^2} + \frac{1}{5} \frac{\partial^2 R_{yyx}^f}{\partial x^2} + \frac{1}{15} \frac{\partial R_{yyx}^{ddf}}{\partial x} + \frac{2}{5} \frac{\partial^2 R_{yyy}^f}{\partial y \partial x} - \frac{2}{15} \frac{\partial R_{yyz}^{df}}{\partial x} + \frac{1}{3} \frac{\partial R_{yzy}^{df}}{\partial y} - \frac{2}{15} \frac{\partial R_{yzy}^{df}}{\partial x} + \frac{2}{15} \frac{\partial^2 R_{yzz}^f}{\partial y \partial x} + \frac{8}{15} \frac{\partial R_{zxx}^{df}}{\partial x} + \frac{1}{3} \frac{\partial R_{zxy}^{df}}{\partial y} - \frac{4}{15} R_{zzz}^{ddf} + \frac{1}{5} \frac{\partial^2 R_{zzz}^f}{\partial x^2} + \frac{1}{15} \frac{\partial^2 R_{zzz}^f}{\partial y^2} + \frac{2}{15} \frac{\partial^2 R_{zzy}^f}{\partial y \partial x} - \frac{2}{5} \frac{\partial R_{zzz}^{df}}{\partial x} - \left(\frac{\partial^2 N_x^{pf}}{\partial y^2} + \frac{\partial^2 N_y^{pf}}{\partial y \partial x} - \frac{\partial^2 N_z^{pf}}{\partial x} \right) = J_1 \frac{\partial^2 u_0}{\partial t^2} - I_4 \frac{\partial^3 w}{\partial x \partial t^2} + I_5 \frac{\partial^2 \phi}{\partial t^2}, \tag{31}$$

$$\delta\psi^{(i)} = \frac{\partial R_{yy}}{\partial y} + \frac{\partial R_{xy}}{\partial x} - Q_y - \frac{1}{2} \frac{\partial N_{xx}^{mdf}}{\partial x} - \frac{1}{2} \frac{\partial N_{xy}^{mdf}}{\partial y} - \frac{1}{2} \frac{\partial^2 N_{xyx}^{mf}}{\partial x^2} - \frac{1}{2} \frac{\partial^2 N_{yzy}^{mf}}{\partial y \partial x} + \frac{1}{2} N_{xz}^{mddf} + \left(\frac{2}{5} \frac{\partial^2 R_{xxx}^f}{\partial y \partial x} - \frac{4}{15} \frac{\partial^2 R_{xxy}^f}{\partial x^2} + \frac{1}{5} \frac{\partial^2 R_{xxy}^f}{\partial y^2} + \frac{1}{15} R_{xxy}^{ddf} - \frac{2}{15} \frac{\partial R_{xxz}^{df}}{\partial y} - \frac{4}{15} \frac{\partial^2 R_{xyx}^f}{\partial x^2} + \frac{1}{5} \frac{\partial^2 R_{xyx}^f}{\partial y^2} + \frac{1}{15} R_{xyx}^{ddf} + \frac{8}{15} \frac{\partial^2 R_{xyy}^f}{\partial y \partial x} + \frac{1}{3} \frac{\partial R_{xyz}^{df}}{\partial x} + \frac{2}{15} \frac{\partial^2 R_{xzz}^f}{\partial x \partial y} + \frac{1}{3} \frac{\partial R_{xzy}^{df}}{\partial x} + \frac{2}{15} \frac{\partial R_{yxx}^f}{\partial x} - \frac{4}{15} \frac{\partial^2 R_{yxx}^f}{\partial x^2} + \frac{1}{5} \frac{\partial^2 R_{yxx}^f}{\partial y^2} + \frac{1}{15} R_{yxx}^{ddf} - \frac{8}{15} \frac{\partial^2 R_{yxy}^f}{\partial y \partial x} + \frac{1}{3} \frac{\partial R_{yxz}^{df}}{\partial x} - \frac{8}{15} \frac{\partial^2 R_{yyx}^f}{\partial y \partial x} - \frac{2}{5} \frac{\partial R_{yyy}^f}{\partial y} + \frac{1}{5} \frac{\partial^2 R_{yyy}^f}{\partial x^2} + \frac{8}{15} \frac{\partial R_{yyz}^{df}}{\partial y} + \frac{1}{3} \frac{\partial R_{yzy}^{df}}{\partial x} + \frac{8}{15} \frac{\partial R_{yzy}^{df}}{\partial y} - \frac{4}{15} R_{yzz}^{ddf} + \frac{1}{5} \frac{\partial^2 R_{yzz}^f}{\partial y^2} + \frac{1}{15} \frac{\partial^2 R_{yzz}^f}{\partial x^2} - \frac{2}{15} \frac{\partial R_{zxx}^{df}}{\partial y} + \frac{1}{3} \frac{\partial R_{zxy}^{df}}{\partial x} + \frac{2}{15} \frac{\partial R_{zzy}^f}{\partial x \partial y} + \frac{1}{3} \frac{\partial R_{zxy}^{df}}{\partial x} - \frac{8}{15} \frac{\partial R_{zzy}^{df}}{\partial y} - \frac{4}{15} R_{zzy}^{ddf} + \frac{1}{5} \frac{\partial^2 R_{zzy}^f}{\partial y^2} + \frac{1}{15} \frac{\partial^2 R_{zzy}^f}{\partial x^2} - \frac{2}{5} \frac{\partial R_{zzz}^{df}}{\partial y} - \left(\frac{\partial^2 N_y^{pf}}{\partial y^2} + \frac{\partial^2 N_z^{pf}}{\partial y \partial x} - \frac{\partial^2 N_x^{pf}}{\partial y} \right) = I_3 \frac{\partial^2 v_0}{\partial t^2} - I_4 \frac{\partial^3 w}{\partial y \partial t^2} + I_5 \frac{\partial^2 \psi}{\partial t^2}, \tag{32}$$

where the resultant loads and moment of inertias can be defined as

$$(N_{ij}, M_{ij}, N_{ij}^f) = \int_{-\frac{h}{2}}^{\frac{h}{2}} \sigma_{ij}(1, z, f(z)) dz \tag{33}$$

$i, j = x, y$

$$(N_{ij}^m, N_{ij}^{mf}, N_{ij}^{mddf}, N_{ij}^{mddf}) = \int_{-\frac{h}{2}}^{\frac{h}{2}} m_{ij} \left(1, f(z), \frac{df(z)}{dz}, \frac{d^2f(z)}{dz^2} \right) dz \tag{34}$$

$i, j = x, y, z$

$$(R_{ijk}, R_{ijk}^z, R_{ijk}^f, R_{ijk}^{df}, R_{ijk}^{ddf}) = \int_{-\frac{h}{2}}^{\frac{h}{2}} \tau_{ijk} \left(1, z, f(z), \frac{df(z)}{dz}, \frac{d^2f(z)}{dz^2} \right) dz \tag{35}$$

$i, j, k = x, y, z$

$$(N_i^p, N_i^p, N_i^{pf}) = \int_{-\frac{h}{2}}^{\frac{h}{2}} P_i(1, z, f(z)) dz \tag{36}$$

$i = x, y$

$$(Q_i) = \int_{-\frac{h}{2}}^{\frac{h}{2}} \sigma_{ij} \left(\frac{df(z)}{dz} \right) dz \quad i = x, y \tag{37}$$

$$(I_0, I_1, I_2, I_3, I_4, I_5) = \int_{-\frac{h}{2}}^{\frac{h}{2}} \rho_i(1, z, z^2, f(z), zf(z), f^2(z)) dz \tag{38}$$

$i = x, y$

3. Solution Procedure

To solve the governing equations of the structure i.e. Eqs. (28)- (32), the Navier approach is utilized. The admissible

displacements and rotation functions that can satisfy all boundary conditions for a simply supported plate are defined as

$$u_0^{(i)} = \sum_{m=1}^{\infty} \sum_{n=1}^{\infty} u_{mn} \cos\left(\frac{m\pi}{a}x\right) \sin\left(\frac{n\pi}{b}y\right) \sin(\lambda_{mn}t) \tag{39}$$

$$v_0^{(i)} = \sum_{m=1}^{\infty} \sum_{n=1}^{\infty} v_{mn} \sin\left(\frac{m\pi}{a}x\right) \cos\left(\frac{n\pi}{b}y\right) \sin(\lambda_{mn}t) \tag{40}$$

$$w^{(i)} = \sum_{m=1}^{\infty} \sum_{n=1}^{\infty} W_{mn} \sin\left(\frac{m\pi}{a}x\right) \sin\left(\frac{n\pi}{b}y\right) \sin(\lambda_{mn}t) \tag{41}$$

$$\phi^{(i)} = \sum_{m=1}^{\infty} \sum_{n=1}^{\infty} \Phi_{mn} \cos\left(\frac{m\pi}{a}x\right) \sin\left(\frac{n\pi}{b}y\right) \sin(\lambda_{mn}t) \tag{42}$$

$$\psi^{(i)} = \sum_{m=1}^{\infty} \sum_{n=1}^{\infty} \Psi_{mn} \sin\left(\frac{m\pi}{a}x\right) \cos\left(\frac{n\pi}{b}y\right) \sin(\lambda_{mn}t) \tag{43}$$

where $(u_{mn}, v_{mn}, W_{mn}, \Phi_{mn}, \Psi_{mn})$ are unknown coefficients, and λ_{mn} denotes the natural frequencies. Substitution of Eqs. (39) - (43) into the Eqs. (28) - (32) leads to the following eigenvalue problem:

$$([K] - \lambda_{mn}^2[M])[\Delta] = 0, \tag{44}$$

in which, [K] and [M] express the stiffness matrix and mass matrix of the system, respectively. Also $[\Delta]$ is the vector of the unknown coefficients. Setting the determinant of the Eq. (44) to zero, eigenvalues and

eigenvectors, which are related to the natural frequencies and mode shapes of the structure are obtained.

4. Discussion

To validate the results, The eigen problem (44) was solved to obtain the natural frequencies of a graphene sheet. A comparison study was made between the present exponential shear deformation results and those reported by the Navier solution [39] for a rectangular nanoplate embedded in an elastic medium.

These results are listed in Table 2 for a square double-layered GS based on the strain gradient, couple stress, and the classical model, respectively. The mechanical properties for each layer of graphene sheets are chosen from Ref. [39], in which length $a=10$ nm, width $b=10$ nm, and the initial interlayer separation between the two adjacent layers is assumed to be $h=0.34$ nm. The van der Waals interaction coefficients $C_{12}=C_{21}=C$ are calculated using Eq. (25), and all the three material length scale parameters are equal to the amount of l , that is $l_0 = l_1 = l_2 = l$.

Besides, Young’s modulus, Poisson’s ratio, and density of each layer are assumed to be $E=1.02$ TPa, $\nu = 0.16$, and $\rho = 2250$ kg/m³, respectively. The natural frequencies of the modified strain gradient theory (MSGT), modified couple stress theory (MCST), and classical plate theory (CPT) with $l = 0.176 \times 10^{-9}$ are obtained for $m=1$ and $n= 1, 2, 3$, in Table 2. As seen, a very good agreement can be observed. According to this table, there is a bit difference among results, which is due to the various shear deformation theories. These differences are created because function $f(z)$ has different expansion through thickness in various theories.

From Table 2, it can be also seen that the natural frequency changes significantly as the mode number rises, which shows that the effect of the mode order on the natural frequency is not negligible. In another validation study, the fundamental frequency of a single layered graphene sheet was compared with that of our model for different values of length scale parameter and aspect ratio using MCST. As observed, again excellent agreement is seen.

Table 1. The van der Waals interaction coefficients c_{ij} (Gpa⁻¹) for a ten-layered GS

N	j=1	j=2	j=3	j=4	j=5	j=6	j=7	j=8	j=9	j=10
i=1	0	-108.6	1.8720	0.1688	0.0301	0.0079	0.0026	0.0010	0.0004	0.0004
i=2	-108.6	0	-108.6	1.8720	0.1688	0.0301	0.0079	0.0026	0.0010	0.0004
i=3	1.8720	-108.6	0	-108.6	1.8720	0.1688	0.0301	0.0079	0.0026	0.0010
i=4	0.1688	1.8720	-108.6	0	-108.6	1.8720	0.1688	0.0301	0.0079	0.0026
i=5	0.0301	0.1688	1.8720	-108.6	0	-108.6	1.8720	0.1688	0.0301	0.0079
i=6	0.0079	0.0301	0.1688	1.8720	-108.6	0	-108.6	1.8720	0.1688	0.0301
i=7	0.0026	0.0079	0.0301	0.1688	1.8720	-108.6	0	-108.6	1.8720	0.1688
i=8	0.0010	0.0026	0.0079	0.0301	0.168	1.872	-108.6	0	-108.6	1.8720
i=9	0.0004	0.0010	0.0026	0.0079	0.030	0.1688	1.8720	-108.6	0	-108.6
i=10	0.000	0.0004	0.00105	0.00265	0.0079	0.03012	0.16889	0.16889	-108.6	0

Table 2. Natural frequencies of a square double-layerd GS with $b= 10$ nm using MSGT, MCST and CPT in the first nine modes ($l = 0.176 \times 10^{-9}, \bar{K}_G=0, \bar{K}_w = 0$)

m	n	Method	ω_1^{MSGT} (THZ)	ω_2^{MSGT} (THZ)	ω_1^{MCST} (THZ)	ω_2^{MCST} (THZ)	ω_1^{CPT} (THZ)	ω_2^{CPT} (THZ)
1	1	ESDT	0.1543	2.4194	0.1017	2.4152	0.0663	2.4137
		TSDT	0.1543	2.4195	0.1018	2.4152	0.0663	2.4138
		Navier[39]	0.1895	2.6888	0.1165	2.6846	0.0690	2.6830
1	2	ESDT	0.3898	2.4446	0.2534	2.2949	0.1648	2.0820
		TSDT	0.3899	2.4447	0.2534	2.2951	0.1648	2.0821
		Navier[39]	0.4742	2.7237	0.2911	2.6979	0.1725	2.6877
1	3	ESDT	0.7794	2.5471	0.5043	2.3321	0.3267	2.1873
		TSDT	0.7794	2.5471	0.5043	2.3321	0.3267	2.1874
		Navier[39]	0.9499	2.8454	0.5823	2.7446	0.3450	2.6877

The natural frequencies of MSGT, MCST, and CPT with $l = 0.176 \times 10^{-9}$ for a double-layered graphene sheet are listed in Table 4 for different foundation parameters and aspect ratios.

Furthermore, Figs 2-5 are plotted for a better understanding of the effect of different parameters on natural frequencies using MSGT, MCST, and CPT. As seen in Table 4, The natural frequency values decline with a growth in the aspect ratio. This is because the graphene sheet considered here is simply supported at all edges, and a decrease in width at a constant length leads to the decrease of degrees of freedom (DOF). Consequently, this causes a decline in stiffness and natural frequency.

Table 5 shows the natural frequencies for double, triple, and five-layered square nano-graphene sheets when $b = 10$ nm and $l = 0.176 \times 10^{-9}$.

As can be seen in Table 5, the natural frequency (ω_1) is independent of the van der Waals interactions. However, all other higher natural frequencies from ω_2 to ω_5 depend on the van der Waals interactions for different numbers

of layers calculated by CPT, the MSGT, and the MCST. This happens because the equations of motion are coupled to each other by the van der Waals interaction coefficients although the effect of the van der Waals interaction does not exist in the fundamental frequency (ω_1).

Figure 2 depicts the impacts of small-scale parameter on the frequency ratio of a double-layered nano-graphene sheet. What stands out here is that the frequency ratio is more significant in lower values of thickness-to- small-scale parameter ratio. This is due to the fact that when the structure is smaller, the influence of size effects is more notable. Figure 3 demonstrates the variation of fundament frequency of a double-layered nano-graphene sheet using MSGT, MCST, and CPT. As plotted, MSGT has the highest and CPT has the lowest eigenvalue, indicating that strain gradient tensors rise the overall stiffness of the structure. It can be also concluded that when structure thickness is more than ten times of the small-scale parameter, results obtained by MSGT and MCST converge to those of CPT.

Table 3. Comparison study for natural frequencies of a graphene sheet with $b= 10$ nm and $h=0.34$ nm

Method	a/b	l		
		0.5h	h	2h
Ref [44]	1	1.0528	1.1974	1.6537
Present		1.0461	1.1861	1.6208
Ref [44]	2	1.0236	1.0915	1.3286
Present		1.0141	1.0832	1.3014
Ref [44]	3	1.0191	1.0744	1.2718
Present		1.0086	1.0624	1.2596

Table 4. Natural frequencies using MSGT, MCST and CPT for various Winkler modulus \bar{K}_w , shear modulus \bar{K}_G , and aspect ratios ($h = 0.34$ nm, $b = 10$ nm, $l = 0.176 \times 10^{-9}$, $m=1$).

n	$K_G(\frac{N}{M})$	a/b	ω_1^{CPT} (THZ)		ω_2^{CPT} (THZ)		ω_1^{MCST} (THZ)		ω_2^{MCST} (THZ)		ω_1^{MSGT} (THZ)		ω_2^{MSGT} (THZ)	
			1014	1017	1014	1017	1014	1017	1014	1017	1014	1017	1014	1017
\bar{K}_w														
1	0	1	0.9884	0.9884	2.6754	2.6738	0.9892	0.9892	2.6757	2.6756	0.9908	0.9908	2.6782	2.688
		2	0.2328	0.2406	2.6660	2.6653	0.1308	0.1443	2.6730	2.6722	0.2689	0.2564	0.2635	1.5305
	5	1	0.1648	0.1531	2.6811	2.6805	0.2534	0.2460	2.6880	2.6874	0.3883	0.3835	2.7042	2.7036
		2	0.0663	0.0256	2.6806	2.6799	0.1017	0.0998	2.6818	2.6817	0.1534	0.1407	2.6842	2.6835
2	0	1	1.5629	1.5628	2.6676	2.6670	1.5658	1.5658	2.7458	2.7451	2.7974	2.7968	3.4675	3.4675
		2	0.1655	0.1540	2.666	2.6652	0.6722	0.6695	2.6729	2.6728	1.2052	0.2564	2.6892	2.6885
	5	1	0.5487	0.5454	2.7184	2.7177	0.8518	0.8496	2.7951	2.7945	1.3140	1.3425	2.9388	2.9388
		2	0.1648	0.1531	2.6812	2.6805	0.2534	0.2527	2.6881	2.6880	0.3883	0.3835	2.7042	2.7036
3	0	1	2.2102	2.2102	3.4104	2.6591	1.6533	1.6522	3.4104	3.4104	2.69021	2.6895	3.7736	3.7731
		2	0.8661	0.8640	2.7818	2.7811	0.3040	0.3034	3.1167	3.1161	0.6652	0.6624	3.4675	3.4675
	5	1	1.1565	1.1550	3.4104	2.8847	1.8220	1.8211	3.4104	3.4104	1.2635	1.2036	3.8507	3.8503
		2	0.3267	0.3209	2.8854	2.6894	0.5043	0.504	3.2094	3.2088	0.7775	0.7751	2.9233	2.9227

Table 5. Comparison of natural frequencies (THz) between double-, triple- and eight-layered square graphene sheets with width $b = 10$ nm, $m=1$, $l = 0.176 \times 10^{-9}$, $\bar{K}_w = 10^{17} (\frac{p\alpha}{m})$, and $\bar{K}_G = 5(\frac{N}{M})$.

N	Natural frequencis (THz)	CPT			MCST			MSGT		
		n=1	n=2	n=3	n=1	n=2	n=3	n=1	n=2	n=3
2	ω_1	0.0256	0.1531	0.3209	0.0812	0.246	0.0501	0.1407	0.3835	0.7751
	ω_2	2.6799	2.6805	3.4104	2.6811	2.6874	3.4104	2.6835	2.7037	3.4675
3	ω_1	0.0256	0.1531	0.3209	0.0813	0.246	0.5007	0.1407	0.3835	0.7751
	ω_2	1.8622	1.8657	1.8829	1.8638	1.8756	1.9217	1.8673	1.8986	2.0109
	ω_3	3.2822	3.2810	3.2859	3.2831	3.2867	3.3083	3.2851	3.3000	3.3613
5	ω_1	0.0256	0.1531	0.3209	0.0812	0.246	0.0501	0.1407	0.3835	0.7751
	ω_2	1.4859	1.1403	1.1723	1.1342	1.1565	1.2337	1.1403	1.1933	1.3684
	ω_3	1.8717	1.8736	2.1986	1.8394	1.9444	2.2394	1.5305	2.2203	2.3156
	ω_4	2.2579	2.4782	3.3253	3.0488	2.5877	2.4305	2.9846	3.0704	3.1352
	ω_5	3.0485	3.6587	3.4963	3.6013	2.6638	3.1844	3.1457	3.3224	3.6706

The influences of aspect ratio and mode numbers on the vibrational behavior of a double-layered nano-graphene sheet are shown in Figures 3 and 4. From Figure 4, it is observed that natural frequency increases by increasing of aspect ratio. Additionally, as seen, the impacts of size effects get less and less by decreasing of aspect ratio. This is because, for a constant length of the nano-graphene sheet, the width of nano-graphene sheet gets smaller by increasing the aspect ratio. On the other hand, it is obvious that the dynamic behavior of a nano-graphene sheet is considerably dependent on its dimensions. Hence, as this figure depicts, the size effects are more notable for higher aspect ratios. Figure 5 demonstrates the variations of mode numbers on natural frequencies. As seen, natural frequencies increase by rising mode number. This is because motions in higher modes need more energy and the structure needs to be stiffer.

5. Conclusion

In this paper, the vibration response of a multi-layered nano-graphene sheet mounted on an elastic medium was studied based on the strain gradient elasticity theory using the exponential shear deformation theory. The model includes three material length scale parameters, which may effectively include the size effect. The model can also cover the modified couple stress plate model or the classical plate model, by setting two or all of the material length scale parameters equal to zero. In the exponential shear deformation theory, an

exponential function is applied in terms of thickness coordinate to include the effect of transverse shear stress and rotary inertia.

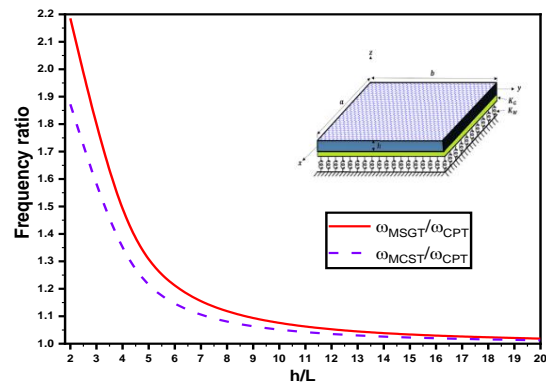


Figure 2. Effects of length scale ratio on frequency ratio of a double-layered nano-graphene sheet

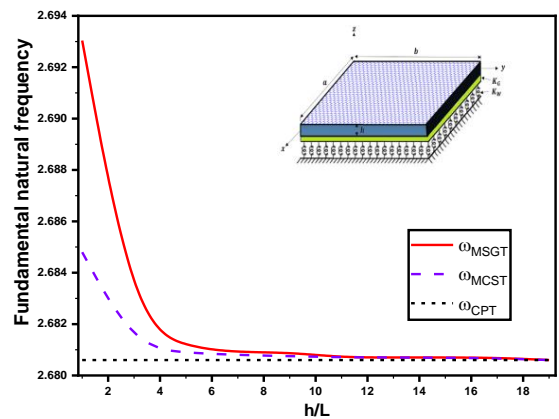


Figure 3. Effects of length scale ratio on fundament frequency of a double-layered nano-graphene sheet using MSGT, MCST, and CPT

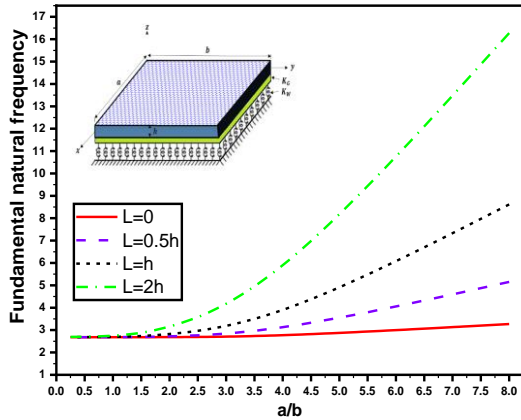


Figure 4. Effects of aspect ratio on fundament frequency of a double-layered nano-graphene sheet using MSGT

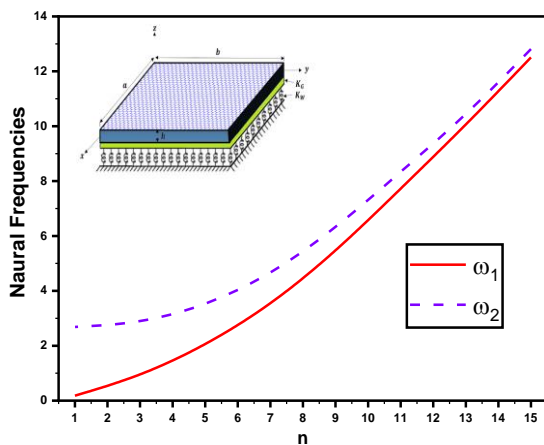


Figure 5. Effects of mode number on natural frequencies of a double-layered nano-graphene sheet using MSGT

The nested nano plates react with each other through the van der Waals interaction between all layers. The equations of motion were derived using Hamilton’s principle. Comparison between the present results and those reported in the literature for simply supported multi-layered nanographene sheets shows high stability and accuracy of the present Navier method. The presented results show the effect of variations of the aspect ratio a/b , Winkler modulus \bar{K}_w , shear modulus \bar{K}_G and size effects on the natural frequency of size-dependent multi-layered nanographene sheets. The results of the present work can be used as benchmarks for future studies.

References

[1] Ghasemi AR., and Mohandes M., 2020. Free vibration analysis of micro and nano fiber-metal laminates circular cylindrical shells based on modified couple stress theory. *Mechanics of Advanced Materials and Structures*, 27(1), pp. 43-54.
 [2] Karimi M., Khorshidi K., Dimitri R., and Tornabene F., 2020. Size-dependent hydroelastic vibration of FG microplates

partially in contact with a fluid. *Composite Structures*, 244, pp. 112320.

[3] McFarland AW., and Colton JS., 2005. Role of material microstructure in plate stiffness with relevance to microcantilever sensors. *Journal of Micromechanics and Microengineering*, 15(5), pp. 1060.
 [4] Khorshidi K., Ghasemi M., Karimi M., and Bahrami M., 2019. Effects of Couple-stress Resultants on Thermo-electro-mechanical Behavior of Vibrating Piezoelectric Microplates Resting on Orthotropic Foundation. *Journal of Stress Analysis*, 4(1), pp. 125-36.
 [5] Lam DC., Yang F., Chong A., Wang J., and Tong P., 2003. Experiments and theory in strain gradient elasticity. *Journal of the Mechanics and Physics of Solids*, 51(8), pp. 1477-508.
 [6] Khorshidi K., Bahrami M., Karimi M., Ghasemi M., 2020. A theoretical approach for flexural behavior of FG vibrating microplates with piezoelectric layers considering a hybrid length scale parameter. *Journal of Theoretical and Applied Vibration and Acoustics*, 6(1), pp. 51-68.
 [7] Khorshidi K., and Karimi M., 2019. Analytical Approach for Thermo-electro-mechanical Vibration of Piezoelectric Nanoplates Resting on Elastic Foundations based on Nonlocal Theory. *Mechanics of Advanced Composite Structures* ,6(2), pp. 117-129.
 [8] Mohandes M., and Ghasemi AR., 2019. A new approach to reinforce the fiber of nanocomposite reinforced by CNTs to analyze free vibration of hybrid laminated cylindrical shell using beam modal function method. *European Journal of Mechanics-A/Solids*, 73, pp. 224-234.
 [9] Khorshidi K., and Karimi M., 2019. Analytical modeling for vibrating piezoelectric nanoplates in interaction with inviscid fluid using various modified plate theories. *Ocean Engineering*, 181, pp. 267-280.
 [10] Soltannia B., Mertiny P., and Taheri F., 2020. Static and dynamic characteristics of nano-reinforced 3D-fiber metal laminates using non-destructive techniques. *Journal of Sandwich Structures & Materials*, 23(7), pp. 3081-112.
 [11] Abbasion S., Rafsanjani A., Avazmohammadi R., and Farshidianfar A., 2009. Free vibration of microscaled Timoshenko beams. *Applied Physics Letters*, 95(14), pp. 143122.
 [12] Alisafaei F., Ansari R., and Rouhi H., 2011. Continuum modeling of van der Waals interaction force between carbon nanocones and carbon nanotubes. *Journal of*

- Nanotechnology in Engineering and Medicine*, 2(3), pp. 031002.
- [13] Jam JE., Mirzaei Y., Gheshlaghi B., and Avazmohammadi R., 2012. Size-dependent free vibration analysis of infinite nanotubes using elasticity theory. *Journal of Mechanics of Materials and Structures*, 7(2), pp. 137-44.
- [14] Koiter W., 1964. Couple-stress in the theory of elasticity. *Proc K Ned Akad Wet*, North Holland Pub.
- [15] Mindlin R., and Tiersten H., 1962. Effects of couple-stresses in linear elasticity. *Archive for Rational Mechanics and Analysis*, 11(1), pp. 415-48.
- [16] Toupin RA., 1962. Elastic materials with couple-stresses. *Archive for Rational Mechanics and Analysis*, 11(1), pp. 385-414.
- [17] Khorshidi K., Karimi M., Bahrami M., Ghasemi M., and Soltannia B., 2022. Fluid-structure interaction analysis of vibrating microplates in interaction with sloshing fluids with free surface. *Applied Ocean Research*, 121, pp. 103088.
- [18] Eringen AC., 1972. Nonlocal polar elastic continua. *International journal of engineering science*, 10(1), pp. 1-16.
- [19] Pradhan S., and Kumar A., 2010. Vibration analysis of orthotropic graphene sheets embedded in Pasternak elastic medium using nonlocal elasticity theory and differential quadrature method. *Computational Materials Science*, 50(1), pp. 239-245.
- [20] Khorshidi K., Karimi M., and Amabili M., 2020. Aeroelastic analysis of rectangular plates coupled to sloshing fluid. *Acta Mechanica*, 231(8), pp. 3183-98.
- [21] Pradhan S., and Murmu T., 2009. Small scale effect on the buckling of single-layered graphene sheets under biaxial compression via nonlocal continuum mechanics. *Computational materials science*, 47(1), pp. 268-74.
- [22] Khorshidi K., and Karimi M., 2020. Fluid-Structure Interaction of Vibrating Composite Piezoelectric Plates Using Exponential Shear Deformation Theory. *Mechanics of Advanced Composite Structures*, 7(1), pp. 59-69.
- [23] Fleck N., and Hutchinson J., 1993. A phenomenological theory for strain gradient effects in plasticity. *Journal of the Mechanics and Physics of Solids*, 41(12), pp. 1825-57.
- [24] Lam DC., Yang F., Chong A., Wang J., and Tong P., 2003. Experiments and theory in strain gradient elasticity. *Journal of the Mechanics and Physics of Solids*. 2003; 51(8); pp. 1477-508.
- [25] Wang M., Yan C., Ma L, Hu N., and Chen M., 2012. Effect of defects on fracture strength of graphene sheets. *Computational Materials Science*, 54, pp. 236-9.
- [26] Ahmadi-Moghadam B., Soltannia B., and Taheri F., 2013. Taheri F., 2013. Interlaminar crack detection in graphene nanoplatelet/CFRP composites using electric resistance change. *Proc 19th Int Conf Compos Mater*; Montreal, Canada Volume: 6.
- [27] Mohandes M., Ghasemi AR., Irani-Rahagi M., Torabi K., and Taheri-Behrooz F., 2018. Development of beam modal function for free vibration analysis of FML circular cylindrical shells. *Journal of Vibration and Control*, 24(14), pp. 3026-35.
- [28] Ansari R., Arash B., and Rouhi H., 2011. Vibration characteristics of embedded multi-layered graphene sheets with different boundary conditions via nonlocal elasticity. *Composite Structures*, 93(9), pp. 2419-29.
- [29] Jafari B., Hakim S., and Nouri M., 2018. Cured Poly (ethylene-g-maleic anhydride) /Graphene Nanocomposite: Properties and Characterization. *Mechanics of Advanced Composite Structures*, 5(1), pp. 1-12.
- [30] Ghasemi AR., and Mohandes M., 2019. Free vibration analysis of rotating fiber-metal laminate circular cylindrical shells. *Journal of Sandwich Structures & Materials*, 21(3), pp. 1009-31.
- [31] Ansari R., Rajabiehfarid R., and Arash B., 2010. Nonlocal finite element model for vibrations of embedded multi-layered graphene sheets. *Computational Materials Science*, 49(4), pp. 831-8.
- [32] Sobhy M., 2016. Hygrothermal vibration of orthotropic double-layered graphene sheets embedded in an elastic medium using the two-variable plate theory. *Applied Mathematical Modelling*, 40(1), pp. 85-99.
- [33] Wang Y-Z., Li F-M., and Kishimoto K., 2011. Thermal effects on vibration properties of double-layered nanoplates at small scales. *Composites Part B: Engineering*, 42(5), pp. 1311-7.
- [34] Shafiei Z., Sarrami-Foroushani S., Azhari F., and Azhari M., 2020. Application of modified couple-stress theory to stability and free vibration analysis of single and multi-layered graphene sheets. *Aerospace Science and Technology*, 98, pp. 105652.
- [35] Karličić D., Čajić M., Kozić P., and Pavlović I., 2015. Temperature effects on the vibration and stability behavior of multi-layered graphene sheets embedded in an elastic medium. *Composite Structures*, 131, pp. 672-81.

- [36] Kitipornchai S., He X., and Liew K., 2005. Continuum model for the vibration of multilayered graphene sheets. *Physical Review B*, 72(7), pp. 075443.
- [37] Hosseini-Hashemi Sh., Mehrabani H., and Ahmadi-Savadkoobi A., 2015. Exact solution for free vibration of coupled double viscoelastic graphene sheets by viscoPasternak medium. *Composites Part B: Engineering*, 78, pp. 377-83.
- [38] He X., Kitipornchai S., and Liew K., 2005. Buckling analysis of multi-walled carbon nanotubes: a continuum model accounting for van der Waals interaction. *Journal of the Mechanics and Physics of Solids*, 53(2), pp. 303-26.
- [39] Ansari R., Arash B., and Rouhi H, 2011. Nanoscale vibration analysis of embedded multi-layered graphene sheets under various boundary conditions. *Computational Materials Science*, 50(11), pp. 3091-100.
- [40] Radić N., and Jeremić D., 2017. A comprehensive study on vibration and buckling of orthotropic double-layered graphene sheets under hygrothermal loading with different boundary conditions. *Composites Part B: Engineering*, 128, pp. 182-99.
- [41] Nazemnezhad R., Zare M., and Hosseini-Hashemi Sh., 2018. Effect of nonlocal elasticity on vibration analysis of multi-layer graphene sheets using sandwich model. *European Journal of Mechanics-A/Solids*, 70, pp. 75-85.
- [42] Arefi M., Zamani M., and Kiani M., 2018. Size-dependent free vibration analysis of three-layered exponentially graded nanoplate with piezomagnetic face-sheets resting on Pasternak's foundation. *Journal of Intelligent Material Systems and Structures*, 29(5), pp. 774-786.
- [43] Jomehzadeh E., and Saidi A., 2011. A study on large amplitude vibration of multilayered graphene sheets. *Computational materials science*, 50(3), pp. 1043-1051.
- [44] Akgöz B., and Civalek Ö., 2012. Free vibration analysis for single-layered graphene sheets in an elastic matrix via modified couple stress theory. *Materials & Design*, 42, pp.164-171.